

Multi-qubit Dynamical Decoupling for Enhanced Crosstalk Suppression

Siyuan Niu,^{1,*} Aida Todri-Sanial,^{2,3} and Nicholas T. Bronn^{4,†}

¹*LIRMM, University of Montpellier, France*

²*LIRMM, University of Montpellier, CNRS, France*

³*Eindhoven University of Technology, Eindhoven, Netherlands.*

⁴*IBM Quantum, IBM T. J. Watson Research Center,*

Yorktown Heights, NY 10598, United States of America

(Dated: March 11, 2024)

Dynamical decoupling (DD) is one of the simplest error suppression methods, aiming to enhance the coherence of qubits in open quantum systems. Moreover, DD has demonstrated effectiveness in reducing coherent crosstalk, one major error source in near-term quantum hardware, which manifests from two types of interactions. Static crosstalk exists in various hardware platforms, including superconductor and semiconductor qubits, by virtue of always-on qubit-qubit coupling. Additionally, driven crosstalk may occur as an unwanted drive term due to leakage from driven gates on other qubits. Here we explore a novel staggered DD protocol tailored for multi-qubit systems that suppresses the decoherence error and both types of coherent crosstalk. We develop two experimental setups – an “idle-idle” experiment in which two pairs of qubits undergo free evolution simultaneously and a “driven-idle” experiment in which one pair is continuously driven during the free evolution of the other pair. These experiments are performed on an IBM Quantum superconducting processor and demonstrate the significant impact of the staggered DD protocol in suppressing both types of coherent crosstalk. When compared to the standard DD sequences from state-of-the-art methodologies with the application of X2 sequences, our staggered DD protocol enhances circuit fidelity by 16.9% and 8.5%, respectively, in addressing these two crosstalk types.

I. INTRODUCTION

The inherent noise in near-term quantum computers hinders the demonstration of practical quantum advantage. Recently, a variety of quantum error mitigation techniques have been developed to tackle this challenge, such as zero noise extrapolation (ZNE) [1, 2], probabilistic error cancellation (PEC) [3], and clifford data regression (CDR) [4], which require substantial overhead in quantum resources (such as the number of circuits executed) in order to model the noise and mitigate the resulting error. Quantum error suppression techniques, such as randomized compiling [5], pulse-scaling for Trotterized circuits [6], and dynamical decoupling (DD) [7–9], offer a reduction in error with no additional quantum resources. DD aims to reduce the decoherence error by decoupling the interaction between the quantum system and the environment. This process involves inserting a sequence of gates that compose the identity during the idle period when the qubit is not being used for computation. This entails very little *classical* overhead, as it only requires identifying the idle times and inserting sequences with a pattern of delays between the gates. It makes DD one of the simplest error suppression methods. Numerous DD sequences have been introduced over decades [8, 10–13], leading to performance improvements on various modalities of quantum computers, including superconducting circuits [14–18], trapped ion [19, 20], and neutral atoms [21]. However, these stud-

ies typically focus on a single qubit coupled to its environment (with the exception of Ref. [22]), however quantum computers consist of many qubits coupled to each other. Regarding Ref. [22], the authors studied static ZZ crosstalk to propose a crosstalk-robust dynamical decoupling (CRDD) protocol, similar in pattern those we consider, and demonstrate improved multi-qubit state preservation over standard DD sequences.

Here, we investigate a different multi-qubit DD strategy called *staggered* DD that consists of a standard DD sequence with symmetric free evolution times on one qubit with the same sequence on an adjacent qubit interleaved in time such that the gates occur in the middle of the free evolution times of the original sequence. In addition to suppressing dephasing and single-qubit coherent errors, we show that staggered DD can suppress undesired two-qubit interactions by inverting their direction of rotation in the two-qubit Hilbert space during each of the half-idle times of the gate interleaving. We first provide some theoretical insight for this method, by placing it in context with the usual treatment of DD for general decoherence. We show that this can suppress crosstalk from unwanted ZZ interactions, which can arise both from static coupling between transmon superconducting qubits and driven crosstalk from cross resonance interaction. We then conduct experiments on an IBM quantum computer to explore both static and driven crosstalk. Even though the standard DD sequence has already shown to reduce the decoherence error and crosstalk [18, 23], the experimental results demonstrate that staggered DD performs better than standard (unstaggered) sequences applied naïvely to all qubits.

* siyuan.niu@lirmm.fr

† ntbronn@us.ibm.com

II. THEORETICAL ANALYSIS

The general Hamiltonian representation for an open quantum system is

$$H = H_S + H_B + H_{SB} \quad (1)$$

where H_S and H_B correspond to the system and bath Hamiltonian respectively, while H_{SB} signifies the interaction between the system and the bath. For a single qubit, the general system-bath interaction (taking $\hbar \equiv 1$ throughout)

$$H_{SB} = \sum_{\alpha=x,y,z} \sigma^\alpha \otimes B_\alpha \quad (2)$$

includes both *coherent* and *incoherent* single-qubit errors, where σ^α (B_α) are the Pauli (bath) operators. The objective of dynamical decoupling is to suppress the unwanted error terms of the total Hamiltonian to a certain order. Taking the simplest DD sequence – X2 as an example, a standard X2 sequence is composed of a repetition of

$$q : f_{\tau/2} - \sigma^x - f_\tau - \sigma^x - f_{\tau/2}, \quad (3)$$

for each qubit q , with τ being the interval between pulses for free evolution f , throughout a total idle period of 2τ . The effect of the first σ^x operation transforms the system-bath Hamiltonian to

$$H'_{SB} = (\sigma^x \otimes I_{SB}) H_{SB} (\sigma^x \otimes I_{SB}) \quad (4)$$

so that the free evolution during f_τ is

$$U'_{SB} = e^{-it(\sigma^x \otimes B_x - \sigma^y \otimes B_y - \sigma^z \otimes B_z)}. \quad (5)$$

Ignoring the σ^x term, $H'_{SB} = -H_{SB}$ (i.e., $U'_{SB} = U_{SB}^\dagger$), therefore the Y and Z terms are cancelled to the first order based on the application of the Baker-Campbell-Hausdorff (BCH) formula to the system-bath interaction over the entire evolution time of 2τ . While the X2 sequence leaves the X term unchanged, it can be removed by more complicated DD sequences such as XY4.

Transmons are a common style of superconducting qubit, where the quantum information is encoded in the frequencies of oscillations of Cooper pairs through a Josephson junction [24]. Two fixed-frequency transmons with fixed coupling may be modelled as Duffing oscillators

$$H_{\text{Duff}} = \sum_{i \in \{0,1\}} \left(\omega_i \hat{a}_i^\dagger \hat{a}_i + \frac{\delta_i}{2} \hat{a}_i^\dagger \hat{a}_i (\hat{a}_i^\dagger \hat{a}_i - 1) \right) + J (\hat{a}_0^\dagger + \hat{a}_0) (\hat{a}_1^\dagger + \hat{a}_1) \quad (6)$$

where ω_i and δ_i are the bare transmon frequencies and anharmonicities, respectively, \hat{a}_i^\dagger (\hat{a}_i) are the creation (annihilation) operators for transmon i and J is the coupling strength. This coupling dresses the transmon frequencies and introduces an always-on static ZZ crosstalk

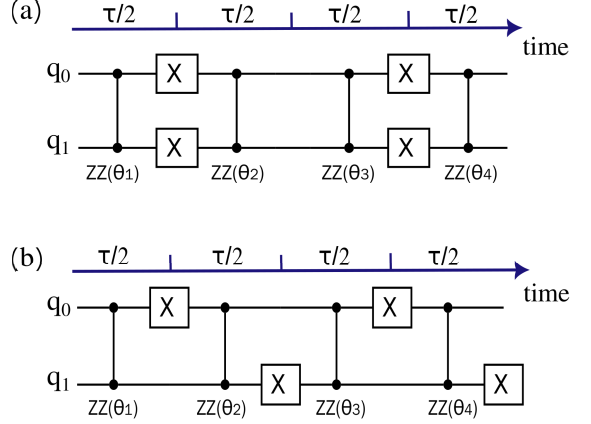


FIG. 1: A quantum circuit evolves an idle period of 2τ and suffers from crosstalk $ZZ(\theta)$, with (a) standard X2 sequence inserted, and (b) staggered X2 sequence inserted.

interaction with strength

$$\begin{aligned} \nu_{ZZ} &= (\omega_{11} - \omega_{01}) - (\omega_{10} - \omega_{00}) \\ &\approx \frac{2J^2(\delta_0 + \delta_1)}{(\delta_1 - \omega_{10} + \omega_{01})(\delta_0 + \omega_{10} - \omega_{01})} \end{aligned} \quad (7)$$

in the perturbative limit where ω_{ij} refers to the energy of the two-qubit state $|ij\rangle$ [25]. Neglecting the system-bath interaction, this generates a coherent rotation in the two-qubit subspace of $ZZ(\theta)$ with $\theta = \nu_{ZZ}t$ where t is the free evolution time. Note that when θ is unspecified, the Pauli operator is assumed (i.e., $\theta = \pi$). This static interaction intrinsically limits quantum volume [26], performance of quantum error correction codes [27], and may prevent scalability of quantum processors [28].

Applying the X2 DD sequence similarly across multiple qubits, the free evolution for each qubit is identical, as XX terms commute with the ZZ crosstalk (we adopt Pauli-string notation, i.e. $XX \equiv \sigma_0^x \otimes \sigma_1^x$, where the position in the string indicates which qubit the Pauli acts on),

$$XX \cdot ZZ(\theta) \cdot XX = ZZ(\theta) \quad (8)$$

thus, the crosstalk accumulates across all the idle times.

$$\begin{aligned} e^{-iZZ\theta_4/2} XX e^{-iZZ(\theta_3+\theta_2)/2} XX e^{-iZZ\theta_1/2} \\ = \exp\{-iZZ(\theta_1 + \theta_2 + \theta_3 + \theta_4)/2\} \end{aligned} \quad (9)$$

If instead, only a single gate were applied to each qubit at a time, the crosstalk can be inverted,

$$XI \cdot ZZ(\theta) \cdot XI = IX \cdot ZZ(\theta) \cdot IX = ZZ(-\theta) \quad (10)$$

The goal of the staggered X2 sequence, in which the DD sequences differ for two qubits (q_0, q_1), is to cancel the accumulated two-qubit ZZ rotation by staggering the timing of the gates in the DD sequences. Specifically,

the X2 staggered sequence

$$\begin{aligned} q_0 : f_{\tau/2} - X - f_{\tau} - X - f_{\tau/2} \\ q_1 : f_{\tau} - X - f_{\tau} - X \end{aligned} \quad (11)$$

creates the free evolution

$$\begin{aligned} IXe^{-iZZ\theta_4/2}XIe^{-iZZ\theta_3/2}IXe^{-iZZ\theta_2/2}XIe^{-iZZ\theta_1/2} \\ = \exp\{-iZZ(\theta_1 - \theta_2 + \theta_3 - \theta_4)/2\} \end{aligned} \quad (12)$$

in which the accumulated phases cancel because each θ_i is an equal rotation over the free evolution time $\tau/2$. An illustration of applying the standard or staggered X2 sequence to a two-qubit circuit is shown in Fig. 1. We can also invert the staggered DD sequences between the control and target qubits to the same effect. This staggered technique can likewise be extended to other DD sequences, such as

$$XY4 = X - Y - X - Y \quad (13)$$

and

$$XY8 = X - Y - X - Y - Y - X - Y - X, \quad (14)$$

where explicit references to the free evolutions f_{τ} have been omitted for simplicity. Noisy simulations illustrating the cancellation of ZZ crosstalk via the use of staggered DD is shown in Appendix C.

In the following, we study the differences between staggered and standard DD sequences of different orders (X2, XY4, XY8) by inserting idle times (representing free evolution of time 2τ) between Clifford gates in two-qubit randomized benchmarking (RB) sequences [29, 30]. These RB sequences are performed individually and in conjunction with operations on an adjacent pair of qubits, and show that staggered DD consistently suppresses coherent error better both when it is caused by static transmon-transmon higher-level coupling and also cross resonance-driven crosstalk.

III. RESULTS

A. Experimental Protocol

We select a subset of nine qubits from the 27-qubit *ibm_cairo* backend, which includes controlled-NOT (CX) pairs generated by both echoed cross resonance (ECR) [31, 32] and direct CX (DCX) [26]. We focus on physically connected qubit pairs due to their increased susceptibility to crosstalk. In this configuration, each pair neighbors the other, where operations on one pair can induce crosstalk in the adjacent pair [33, 34]. We present the RB experiments in two experimental settings: (i) *idle-idle* in which the two pairs of qubits are simultaneously idle during their simultaneous RB sequences (aside from the relevant DD sequences) in Section III B, and (ii) *idle-driven* in which the fidelity of the vulnerable

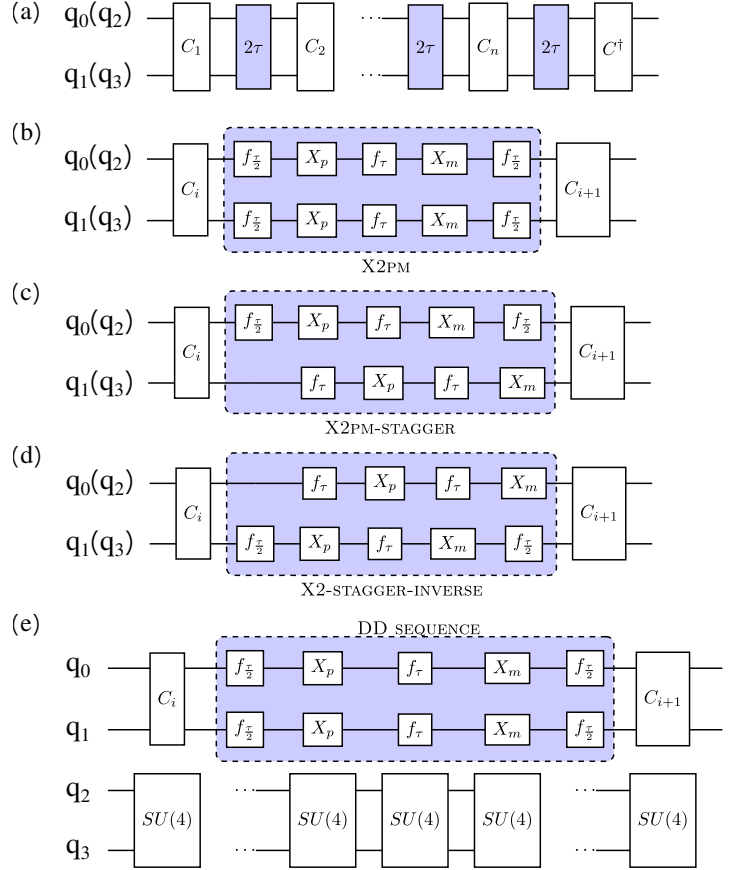


FIG. 2: The RB circuit for a qubit pair is shown in (a). We insert X2pm DD sequence in (b), staggered X2pm sequence in (c) and inverse of staggered X2pm in (d). The circuit for driven-idle experiment composed of RB and SU(4) is shown in (e).

pair of qubits is measured after the RB sequence (with varying DD sequence) while the other pair of qubits is driven by a random sequence of two-qubit gates (SU(4)) in Section III C. The two-qubit *individual* RB circuit sets a baseline for the two experiments for comparison, where the ZZ interaction between qubits in the pair is suppressed by calibrating rotary echo pulses on the target qubits [35]. This is compared to the same RB circuit but while a neighboring is active, effectively exposing the pair to static and/or driven crosstalk (the effect of static crosstalk in which the neighboring qubits are in the ground state has been calibrated out by the backend). The idle-idle and idle-driven experiments expand to involve two qubit pairs, totaling four qubits. Standard and staggered DD sequences are inserted during the idle periods. Specifically, in the idle-idle experiment, DD are applied to both qubit pairs, whereas in the second experiment, DD is only applied to the first qubit pair with RB sequences. These experiments highlight the difference in performance between standard and staggered DD sequences when the qubits are exposed to both stochastic dephasing and coherent crosstalk arising from static ZZ

coupling and cross-resonance driven ZZ . The quantum circuits were generated and executed using the *Qiskit Experiments* framework [36].

In the following experiments, the two-qubit RB circuits consist of a fixed number of Clifford gates (Clifford sequence) and a final sequence separated by varying lengths of the idle period of 2τ ranging from 284.4 ns to 3128.9 ns as shown in Fig. 2a. Note that these idle durations are chosen as multiples of the sampling rate of the pulse waveform generator $dt = 0.22$ ns on *ibm_cairo*. The same Clifford sequence with $n = 8$ gates and an additional Clifford gate C^\dagger is applied to invert all the previous operations to the initial state. This setting maintains a high initial fidelity ($\gtrsim 0.8$) at the minimum idle time. Note that, the circuit depth remains constant throughout the experiment, with the only varying parameter being the length of the delay that separates the sets of Clifford gates.

We choose a pair of qubits (q_{11}, q_{14}) and (q_{12}, q_{13}) for study, that are particularly vulnerable to crosstalk from operations on neighboring qubit pair, as shown by the fidelity differences between Fig. 3a and Fig. 3b. For idle-idle experiment, we apply exactly the same RB circuit simultaneously to the adjacent pair of qubits. While the duration of the idle period remains the same for both qubit pairs, the starting points of these idle periods differ slightly due to the differences in duration of the two neighboring CX pairs. We use the *As Late As Possible* policy to schedule the circuits. For the idle-driven experiment, while one qubit pair undergoes the RB circuit, its adjacent pair is subjected to a circuit composed of different random SU(4) blocks, which continuously drives crosstalk during the RB experiment, as shown in Fig. 2e. The number of SU(4)s in the circuit is determined to make sure that has the same duration as the RB circuit. This experimental arrangement ensures the simultaneous execution of both circuits. Since no idle time is inserted between SU(4)s, during the idle periods of the RB circuit, the neighboring qubits in the SU(4) circuit remain active thereby contributing driven crosstalk.

We measure the probability of return to the initial state (as it is related to the randomized benchmarking protocol), to gauge the fidelity changes across time. Moreover, we numerically calculate the time average fidelity [17, 22],

$$F_{\text{avg}}(t) = \frac{1}{T} \int_0^T dt \frac{F(t)}{F(0)} \quad (15)$$

to indicate the overall fidelity change over time, where $F(t)$ represents the probability of return at time t .

During the idle period, DD sequences implemented in different ways at the pulse and timing level are inserted as depicted in Fig. 2b-d. Standard DD sequences have symmetric timing on both qubits, and they occur simultaneously (see Fig. 2b for a representation of the X2 sequence). For staggered sequences, the sequence on one qubit is symmetric (as in the standard case) and the other is offset such that each staggered pulse occurs

halfway between the symmetric pulses on the other qubit (Fig. 2c). The “inverse” staggered sequence switches the role of symmetric and staggered sequences on the qubits (Fig. 2d). While each sequence is nominally identical from the perspective of unitary operations (composing to the identity), there are control variations at the pulse level [17] that may effect their performance. We consider the default X gate to be a $+\pi$ rotation around the x -axis of the Bloch sphere (also denoted X_p) and X_m a $-\pi$ rotation with negative amplitude at the pulse level. These variations consisting of alternating rotations are denoted with pm after the sequence name. For example, the X2pm sequence consists of the gates $X_p - X_m$.

In the two experiments, the CX gate is aligned with the native direction of either ECR or DCX gates, determined in calibration to that of higher fidelity. For the two adjacent qubit pairs, the neighbor qubits from each pair can be control-control, control-target, or target-target in their respective pairs. The performances across these different configurations, in terms of the type of CX gate and the type of connected neighbor qubits, are detailed in Appendix A.

B. Idle-idle Experiment - Simultaneous Randomized Benchmarking

We evaluate the performances of standard DD sequences, including X2/X2pm, XY4/XY4pm, XY8/XY8pm, and their staggered and inverse of staggered variants - 16 sequences in total. We then compare these sequences to a baseline, in which the qubits remain free evolution during the delay, with no DD sequence inserted as shown in Fig. 2a.

The RB and simultaneous RB (SRB) results for the qubit pair (q_{11}, q_{14}) are illustrated in Fig. 3, showcasing the comparison between various X2 sequences (X2pm, X2pm-stag, X2pm-stag-inv) against the free evolution. In the SRB experiment, it involves the adjacent qubit pair of (q_{11}, q_{14}) , which is (q_{12}, q_{13}) , with q_{14} and q_{13} being the target qubits in their respective pairs and neighboring each other. The figure shows the connectivity of the two qubit pairs, detailing the type of CX gate used (ECR or DCX) and identifying whether a qubit acts as a control (C) or target (T) for the neighboring qubit connections between pairs. The connection between the qubit pair (q_{11}, q_{14}) is highlighted in red to indicate the specific results corresponding to this pair in the figure. The insertion of default X2 pulses results in unexpected behavior, even degrading the performance below that of the free evolution. The reason for this outcome is elaborated in Appendix B.

We also demonstrate the results for XY4 and XY8 sequences in Fig. 4. Given the negligible difference between the results for staggered DD and its inverse, only the staggered DD is depicted. We observe “dropouts” in fidelity for a short idle times in the XY8 sequence which can be explained by constructive interference of

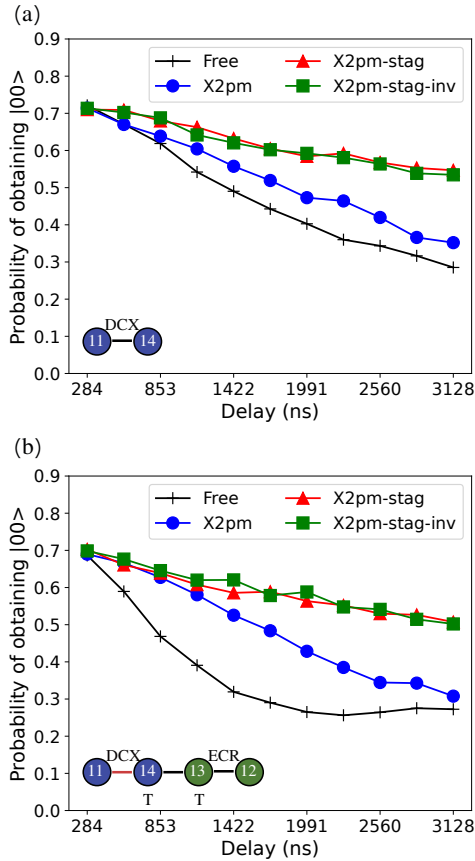


FIG. 3: Free evolution experiment results on qubit pairs (q_{11}, q_{14}) and (q_{12}, q_{13}) when comparing the baseline (free evolution) with different DD sequences: X2pm, X2pm staggered, and X2pm staggered inverse. (a) The probability of yielding $|00\rangle$ for (q_{11}, q_{14}) when RB is applied to this qubit pair in isolation. (b) The same probability when SRB is applied to both qubit pairs.

The significant difference in fidelity during free evolution between the RB and SRB experiments indicates additional crosstalk generated by the neighboring qubit pair.

higher frequency spectral noise components [37, 38]. In addition, the XY8 sequence shows consistently worse results than XY4.. Therefore, our subsequent discussions will focus primarily on the X2 and XY4 sequences. The correlation between the duration of the idle period and various DD sequences is elaborated upon in Appendix ??.

C. Driven-idle Experiment - Randomized Benchmarking and Random SU(4)

In Fig. 5, we present the fidelity results when (1) applying only the RB circuit to (q_{11}, q_{14}) and (2) additionally performing the SU(4) circuit on the adjacent (q_{12}, q_{13}) pair. Again, the qubits neighboring each other across the two pairs are target qubits within their respective pairs.

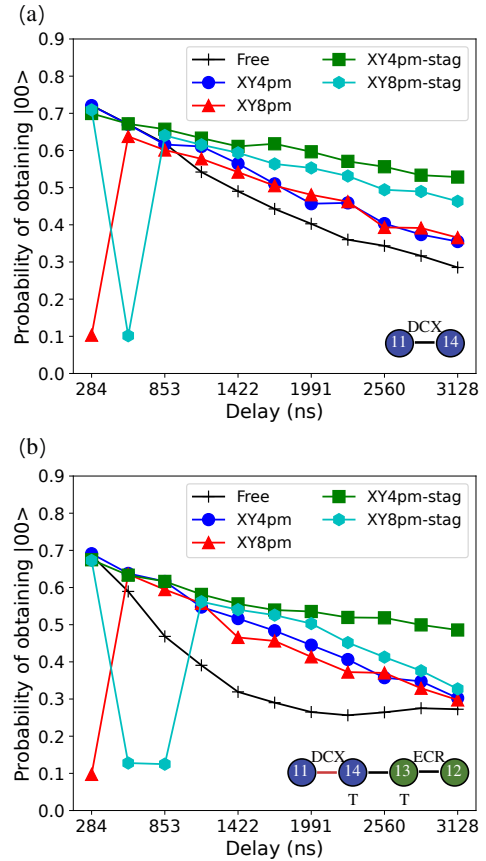


FIG. 4: Free evolution experiment results on qubit pairs (q_{11}, q_{14}) and (q_{12}, q_{13}) when comparing the baseline (free evolution) with XY4pm, XY4pm staggered, XY8pm, and XY8pm staggered. (a) The probability of yielding $|00\rangle$ for (q_{11}, q_{14}) when RB is applied to this qubit pair in isolation. (b) The same probability when SRB is applied to both qubit pairs.

Similar to the free evolution experiment, the staggered DD sequences consistently outperform the non-staggered DD sequences. In comparison to the baseline, we observe a significant enhancement in fidelity for the X2pm, XY4pm, X2pm-stag, and XY4pm-stag sequences when the RB circuit operates independently. This improvement becomes more pronounced when the RB and SU(4) circuits are executed simultaneously.

D. Result Analysis

The time average fidelities F_{avg} for qubit pair (q_{11}, q_{14}) , calculated using Eq. 15 for both idle-idle and driven-idle experiments are shown in Table I. For these experiments, T is set to 3128.9 ns. The RB results provide a baseline comparison for the two experiments. Relative to free evolution, the application of standard X2pm and the better performing variant of staggered X2pm (chosen between X2pm-stag and X2pm-stag-inv) sequences enhances F_{avg}

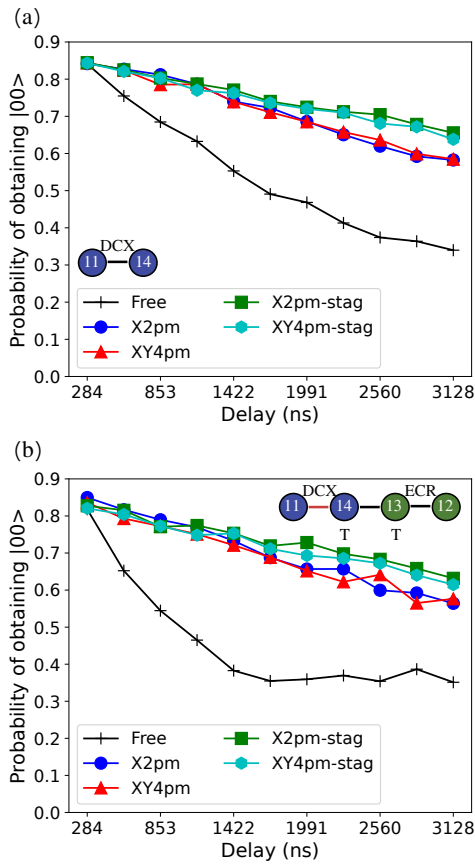


FIG. 5: Crosstalk experiment results on qubit pairs (q_{11}, q_{14}) and (q_{12}, q_{13}) . (a) The probability of yielding $|00\rangle$ for (q_{11}, q_{14}) when only RB is applied. (b) The same probability when of yielding $|00\rangle$ for (q_{11}, q_{14}) when RB is applied to this qubit pair while SU(4) is applied to its adjacent qubit pair (q_{12}, q_{13}) .

TABLE I: Time average fidelity for (q_{11}, q_{14}) when RB is applied and RB/SU(4) is applied to its neighboring qubit pairs (q_{12}, q_{13}) . Note that, the fluctuation of RB results is due to the time difference when submitting the circuits.

Experiments		Free	X2pm	X2pm-stag	X2pm-stag-inv
idle-idle	RB	0.65	0.73	0.88	0.86
	SRB	0.52	0.71	0.83	0.85
driven-idle	RB	0.63	0.85	0.89	0.88
	RB-SU(4)	0.54	0.82	0.89	0.88

by 23.4% and 38.3% on average. In SRB experiment, active neighbor qubit pair generates static crosstalk when it is not in the ground state, reducing the fidelity compared with the RB experiment. Nonetheless, with DD sequences, F_{avg} remains stable showing improvements of 36.5% and 59.6% for standard and staggered X2pm compared with the free evolution. For RB-SU(4) experiment, which introduces both static and driven crosstalk, lead-

ing to a decrease of F_{avg} during free evolution. Here, the standard and staggered X2pm sequences boost F_{avg} by 51.9% and 64.8% compared with the free evolution. Overall, the staggered (inverse) X2pm yield fidelity improvements of 12%, 16.9% and 8.5% over standard X2pm across isolated RB, idle-idle (SRB), and idle-driven (RB-SU(4)) experiments, respectively. The decrease in relative effectiveness in the idle-driven experiment may be due to the twirling effect of crosstalk from random SU(4)s [39].

IV. CONCLUSION

Our proposed staggered DD protocol can be considered as an entry point for integrating DD sequences into multi-qubit quantum systems. Throughout the experiments, we have tailored our staggered DD protocol to fit X2, XY4, and XY8 sequences, incorporating them during unified idle times. Several advanced DD sequences, such as UDD [12] and UR [13], offering opportunities for further exploration. One natural following step is to apply the staggered DD protocol to these sequences and delve into DD scheduling methods for non-unified idle time in large quantum systems. Recently, many efforts are focused on understanding noise models for quantum hardware and developing corresponding error suppression or mitigation techniques [3]. An interesting direction is to synergize the staggered DD protocol with these techniques to enhance circuit fidelity further. Moreover, standard DD sequences have been employed to protect idle qubits for quantum error correction or detection codes [15, 40–42]. Incorporating our staggered DD protocol into quantum error correction codes offers a pathway toward achieving fault-tolerant quantum computing. Despite of the positive impact of DD sequences, challenges such as dropouts or instability across different qubits persist. Additional experiments are necessary to deepen the understanding of hardware noise sources and to devise more hardware-oriented DD sequences.

ACKNOWLEDGMENTS

The authors acknowledge the IBM Quantum Network Hub at QuantUM Initiative of the Region Occitanie and University of Montpellier for providing additional quantum resources through its partnership with IBM. The authors would like to thank Bibek Pokharel for a careful reading of the manuscript and Ali Javadi-Abhari and Petar Jurcevic for insightful discussions.

Appendix A: Various Experimental Configurations

There are two variants of CX gates in IBM quantum hardware: Echoed Cross-Resonance CX (ECR), and Direct CX (DCX). We select several qubit pairs from

ibmq_cairo including both ECR and DCX types, and list their respective amplitudes, duration, and error rates in Table II. Note that, CX gate is natively uni-direction in IBM quantum hardware, and the opposite direction is realized by adding extra single qubit gates. Therefore, we show explicitly the control and target qubits for each qubit pair in the table. Generally, DCX gate exhibits a lower error rate and shorter duration compared with ECR gate. However, DCX gate is more susceptible to crosstalk, as illustrated in Fig. 6. Here, the CNOT error rate, derived from SRB, exhibits a notable increase compared to the rate derived from independent RB for the DCX type of CNOT gate, whereas the CNOT error rate for the ECR CNOT only experiences a slight increase.

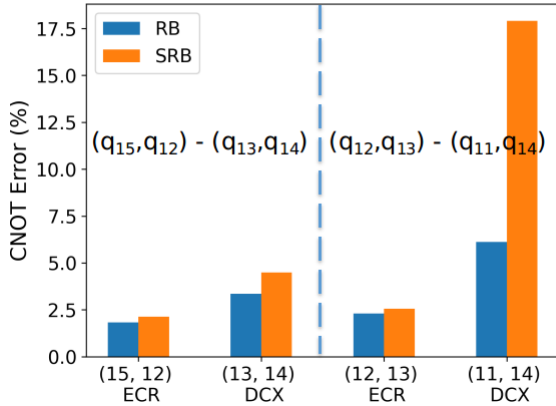


FIG. 6: We perform RB and SRB on two qubit pairs and calculate the corresponding CNOT error rate. The selected qubit pairs employ either ECR or DCX type of

CNOT gate. An increase in the CNOT error rate observed during SRB as compared to RB indicates the impact of crosstalk.

We conduct both idle-idle and driven-idle experiments on adjacent qubit pairs across three distinct scenarios: (DCX, DCX), (ECR, DCX), and (ECR, ECR). Given the adjacency of the two pairs, one qubit from the first pair is positioned next to a qubit from the second pair, following different configurations: control-control, control-target, or target-target. The results of these experiments are displayed in Fig. 7. In the case of driven-idle experiments, staggered DD consistently demonstrates superior performance over standard DD. However, for the idle-idle experiments, the performance of staggered DD exhibits a lack of consistency.

Appendix B: X2

The exploration of circuit fidelity for both idle-idle and driven-idle experiments reveal that the insertion of $X2$ sequence leads to worse outcomes than the baseline, as

shown in Fig. 8, which is potentially due to the imperfections in the X gate. However, this was not reproducible in simulations with an error model informed by quantum process tomography. Rather, we suspect an observation similar to Ref. [17] performed on IBM quantum hardware, where fidelity decreases due to the asymmetry of the trajectory around the Bloch sphere during qubit rotations. Since an X gate corresponds to a π rotation around the x -axis in one direction, this asymmetry accumulates after two consecutive X gates, thereby resulting in poorer performance compared to the baseline where no DD sequence is inserted. On the other hand, the Xp and Xm operations, which correspond to a π rotation around the X axis in opposite directions, effectively mitigate this asymmetry.

Appendix C: Noisy Simulation Results

We utilize a noise simulator to perform a T2 Ramsey experiment, aiming at demonstrating the effectiveness of staggered DD in mitigating the effects of ZZ crosstalk. The noise model exclusively contains thermal relaxation without any gate or readout errors. We set the induced oscillation frequency to 100kHz to enable more precise measurement.

The procedure begins by inserting $X2pm$ along with its staggered counterpart into the delay of the Ramsey experiment. Within these DD-inserted circuits, we incorporate an additional $ZZ(\theta)$ gate prior to each delay, with $\theta = wt$, serving to simulate ZZ crosstalk across time evolution t . We evaluate the discrepancies in detuning frequency when inserting either standard or staggered DD sequences into Ramsey experiment circuits. This comparison is performed under two conditions: with and without the introduction of ZZ crosstalk. The resulting detuning frequencies are detailed in Table III. Staggered DD is shown to be highly effective in suppressing the impacts of ZZ crosstalk, evident in its ability to maintain a consistent detuning frequency in comparison to the non-crosstalk scenario. Conversely, the presence of ZZ crosstalk instigates a frequency shift when inserting standard DD. This noise simulation outcome aligns with the theoretical analysis, validating the capability of staggered DD in canceling out ZZ crosstalk.

CX(control-target)	Type	Amplitude	Duration (dt)	Error rate (%)
(10, 12)	DCX	0.42	1008	0.66
(13, 14)	DCX	0.33	992	0.49
(11, 14)	DCX	0.49	848	1.37
(1, 0)	ECR	0.91	2400	2.57
(4, 7)	ECR	0.58	1184	1.64
(15, 12)	ECR	0.52	2208	0.9
(12, 13)	ECR	0.92	1760	1.4

TABLE II: CX information.

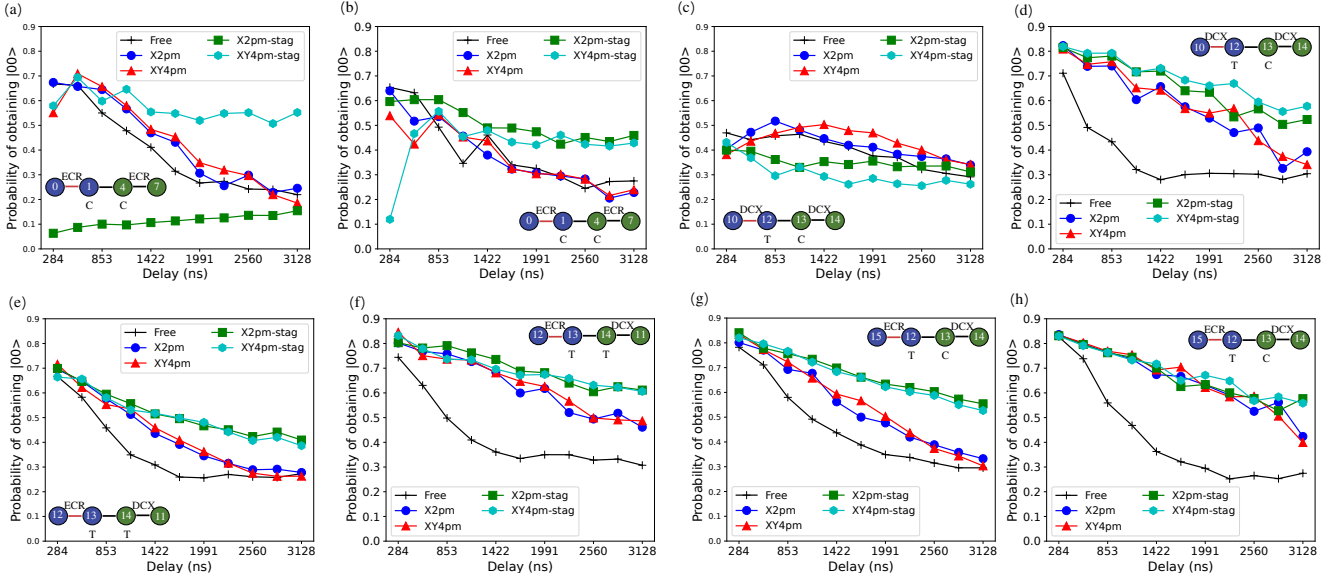


FIG. 7: Free evolution and crosstalk experiment results on pairs $[(q_1, q_0) - (q_4, q_7)]$

are shown in (a) and (b), on $[(q_{10}, q_{12}) - (q_{13}, q_{14})]$ are shown in (c) and (d), on $[(q_{12}, q_{13}) - (q_{11}, q_{14})]$ are shown in (e) and (f), and on $[(q_{15}, q_{12}) - (q_{13}, q_{14})]$ are shown in (g) and (h).

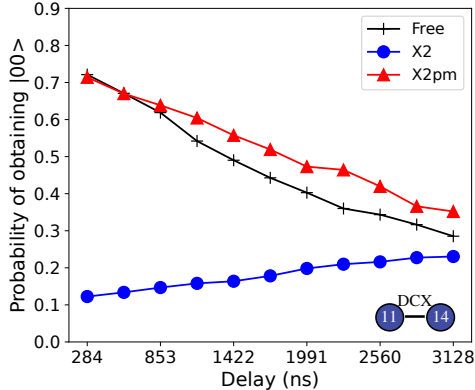


FIG. 8: Comparison between free evolution, X2pm, and X2 pulse when applying RB sequences to (q_{11}, q_{14}) .

- [1] Y. Li and S. C. Benjamin, Efficient variational quantum simulator incorporating active error minimization, *Physical Review X* **7**, 021050 (2017).
- [2] K. Temme, S. Bravyi, and J. M. Gambetta, Error mitigation for short-depth quantum circuits, *Physical review letters* **119**, 180509 (2017).
- [3] E. Van Den Berg, Z. K. Minev, A. Kandala, and K. Temme, Probabilistic error cancellation with sparse pauli-lindblad models on noisy quantum processors, *Nature Physics* , 1 (2023).
- [4] P. Czarnik, A. Arrasmith, P. J. Coles, and L. Cincio, Error mitigation with clifford quantum-circuit data, *Quantum* **5**, 592 (2021).
- [5] J. J. Wallman and J. Emerson, Noise tailoring for scalable

- quantum computation via randomized compiling, *Phys. Rev. A* **94**, 052325 (2016).
- [6] J. P. Stenger, N. T. Bronn, D. J. Egger, and D. Pekker, Simulating the dynamics of braiding of Majorana zero modes using an IBM quantum computer, *Physical Review Research* **3**, 033171 (2021).
- [7] L. Viola and S. Lloyd, Dynamical suppression of decoherence in two-state quantum systems, *Physical Review A* **58**, 2733 (1998).
- [8] L. Viola, E. Knill, and S. Lloyd, Dynamical decoupling of open quantum systems, *Physical Review Letters* **82**, 2417 (1999).
- [9] M. J. Biercuk, H. Uys, A. P. VanDevender, N. Shiga, W. M. Itano, and J. J. Bollinger, Optimized dynamical

TABLE III: T2 Ramsey experiment.

Experimental setup	Detuning frequency (KHz)
X2pm	100
X2pm + ZZ	91.7
Staggered X2pm	100
Staggered X2pm + ZZ	99.1

decoupling in a model quantum memory, *Nature* **458**, 996 (2009).

[10] S. Meiboom and D. Gill, Modified spin-echo method for measuring nuclear relaxation times, *Review of scientific instruments* **29**, 688 (1958).

[11] J. Zhang, A. M. Souza, F. D. Brandao, and D. Suter, Protected quantum computing: interleaving gate operations with dynamical decoupling sequences, *Physical review letters* **112**, 050502 (2014).

[12] G. S. Uhrig, Keeping a quantum bit alive by optimized π -pulse sequences, *Physical Review Letters* **98**, 100504 (2007).

[13] G. T. Genov, D. Schraft, N. V. Vitanov, and T. Halfmann, Arbitrarily accurate pulse sequences for robust dynamical decoupling, *Physical review letters* **118**, 133202 (2017).

[14] S. Niu and A. Todri-Sanial, Effects of dynamical decoupling and pulse-level optimizations on ibm quantum computers, *IEEE Transactions on Quantum Engineering* **3**, 1 (2022).

[15] B. Pokharel and D. A. Lidar, Demonstration of algorithmic quantum speedup, *Physical Review Letters* **130**, 210602 (2023).

[16] A. M. Souza, Process tomography of robust dynamical decoupling with superconducting qubits, *Quantum Information Processing* **20**, 237 (2021).

[17] N. Ezzell, B. Pokharel, L. Tewala, G. Quiroz, and D. A. Lidar, Dynamical decoupling for superconducting qubits: a performance survey, *arXiv preprint arXiv:2207.03670* (2022).

[18] V. Tripathi, H. Chen, M. Khezri, K.-W. Yip, E. Levenson-Falk, and D. A. Lidar, Suppression of crosstalk in superconducting qubits using dynamical decoupling, *Physical Review Applied* **18**, 024068 (2022).

[19] A. Bermudez, P. O. Schmidt, M. B. Plenio, and A. Retzker, Robust trapped-ion quantum logic gates by continuous dynamical decoupling, *Physical Review A* **85**, 040302 (2012).

[20] W. Morong, K. Collins, A. De, E. Stavropoulos, T. You, and C. Monroe, Engineering dynamically decoupled quantum simulations with trapped ions, *PRX Quantum* **4**, 010334 (2023).

[21] D. Bluvstein, H. Levine, G. Semeghini, T. T. Wang, S. Ebadi, M. Kalinowski, A. Keesling, N. Maskara, H. Pichler, M. Greiner, *et al.*, A quantum processor based on coherent transport of entangled atom arrays, *Nature* **604**, 451 (2022).

[22] Z. Zhou, R. Sitler, Y. Oda, K. Schultz, and G. Quiroz, Quantum crosstalk robust quantum control, *arXiv preprint arXiv:2208.05978* (2022).

[23] C. Tong, H. Zhang, and B. Pokharel, Empirical learning of dynamical decoupling on quantum processors (2024), *arXiv:2403.02294 [quant-ph]*.

[24] J. Koch, T. M. Yu, J. M. Gambetta, A. A. Houck, D. I. Schuster, J. Majer, A. Blais, M. H. Devoret, S. M. Girvin, and R. J. Schoelkopf, Charge-insensitive qubit design derived from the Cooper pair box, *Physical Review A* **76**, 042319 (2007).

[25] K. X. Wei, E. Magesan, I. Lauer, S. Srinivasan, D. F. Bogorin, S. Carnevale, G. A. Keefe, Y. Kim, D. Klaus, W. Landers, N. Sundaresan, C. Wang, E. J. Zhang, M. Steffen, O. E. Dial, D. C. McKay, and A. Kandala, Hamiltonian engineering with multicolor drives for fast entangling gates and quantum crosstalk cancellation, *Phys. Rev. Lett.* **129**, 060501 (2022).

[26] P. Jurcevic, A. Javadi-Abhari, L. S. Bishop, I. Lauer, D. F. Bogorin, M. Brink, L. Capelluto, O. Günlük, T. Itoko, N. Kanazawa, A. Kandala, G. A. Keefe, K. Kruslich, W. Landers, E. P. Lewandowski, D. T. McClure, G. Nannicini, A. Narasgond, H. M. Nayfeh, E. Pritchett, M. B. Rothwell, S. Srinivasan, N. M. Sundaresan, C. Wang, K. X. Wei, C. J. Wood, J.-B. Yau, E. J. Zhang, O. E. Dial, J. M. Chow, and J. M. Gambetta, Demonstration of quantum volume 64 on a superconducting quantum computing system, *Quantum Science and Technology* **6**, 025020 (2021).

[27] M. Takita, A. W. Cross, A. D. Córcoles, J. M. Chow, J. M. Gambetta, E. Magesan, B. Abdo, M. Brink, A. W. Cross, J. M. Chow, and J. M. Gambetta, Demonstration of weight-four parity measurements in the surface code architecture, *Physical Review Letters* **119**, 180501 (2017).

[28] C. Berke, E. Varvelis, S. Trebst, A. Altland, and D. P. DiVincenzo, Transmon platform for quantum computing challenged by chaotic fluctuations, *Nature Communications* **13**, 10.1038/s41467-022-29940-y (2022).

[29] E. Magesan, J. M. Gambetta, and J. Emerson, Scalable and Robust Randomized Benchmarking of Quantum Processes, *Physical Review Letters* **106**, 180504 (2011).

[30] E. Magesan, J. M. Gambetta, and J. Emerson, Characterizing quantum gates via randomized benchmarking, *Physical Review A* **85**, 042311 (2012).

[31] J. M. Chow, A. D. Córcoles, J. M. Gambetta, C. Rigetti, B. R. Johnson, J. A. Smolin, J. R. Rozen, G. A. Keefe, M. B. Rothwell, M. B. Ketchen, and M. Steffen, Simple All-Microwave Entangling Gate for Fixed-Frequency Superconducting Qubits, *Physical Review Letters* **107**, 080502 (2011).

[32] S. Sheldon, E. Magesan, J. M. Chow, and J. M. Gambetta, Procedure for systematically tuning up crosstalk in the cross-resonance gate, *Physical Review A* **93**, 060302 (2016).

[33] P. Murali, D. C. McKay, M. Martonosi, and A. Javadi-Abhari, Software mitigation of crosstalk on noisy intermediate-scale quantum computers, *International Conference on Architectural Support for Programming Languages and Operating Systems - ASPLOS* , 1001 (2020), 2001.02826.

[34] E. Wilson, S. Singh, and F. Mueller, Just-in-time Quantum Circuit Transpilation Reduces Noise, *Proceedings - IEEE International Conference on Quantum Computing and Engineering, QCE 2020* , 345 (2020).

[35] N. Sundaresan, I. Lauer, E. Pritchett, E. Magesan, P. Jurcevic, and J. M. Gambetta, Reducing unitary and spectator errors in cross resonance with optimized rotary echoes, *PRX Quantum* **1**, 020318 (2020).

[36] N. Kanazawa, D. J. Egger, Y. Ben-Haim, H. Zhang,

W. E. Shanks, G. Aleksandrowicz, and C. J. Wood, Qiskit Experiments: A Python package to characterize and calibrate quantum computers, *Journal of Open Source Software* **8**, 5329 (2023).

[37] T. Yuge, S. Sasaki, and Y. Hirayama, Measurement of the noise spectrum using a multiple-pulse sequence, *Phys. Rev. Lett.* **107**, 170504 (2011).

[38] S. Kotler, N. Akerman, Y. Glickman, and R. Ozeri, Non-linear single-spin spectrum analyzer, *Phys. Rev. Lett.* **110**, 110503 (2013).

[39] A. Hashim, R. K. Naik, A. Morvan, J.-L. Ville, B. Mitchell, J. M. Kreikebaum, M. Davis, E. Smith, C. Iancu, K. P. O'Brien, I. Hincks, J. J. Wallman, J. Emerson, and I. Siddiqi, Randomized Compiling for Scalable Quantum Computing on a Noisy Superconducting Quantum Processor, *Physical Review X* **11**, 1 (2021).

[40] S. Krinner, N. Lacroix, A. Remm, A. Di Paolo, E. Genois, C. Leroux, C. Hellings, S. Lazar, F. Swiadek, J. Hermann, *et al.*, Realizing repeated quantum error correction in a distance-three surface code, *Nature* **605**, 669 (2022).

[41] D. Bluvstein, S. J. Evered, A. A. Geim, S. H. Li, H. Zhou, T. Manovitz, S. Ebadi, M. Cain, M. Kalinowski, D. Hangleiter, *et al.*, Logical quantum processor based on reconfigurable atom arrays, *Nature* , 1 (2023).

[42] G. Quiroz, B. Pokharel, J. Boen, L. Tewala, V. Tripathi, D. Williams, L.-A. Wu, P. Titum, K. Schultz, and D. Lidar, Dynamically generated decoherence-free subspaces and subsystems on superconducting qubits, *arXiv preprint arXiv:2402.07278* (2024).